Development of 50 W class RF gridded ion thruster

IEPC-2019-383

Presented at the 36th International Electric Propulsion Conference
University of Vienna • Vienna, Austria
September 15-20, 2019

Tr. D. Quang Pham[1], Huong. T.T. Nguyen[2] and Jichul Shin[3]
Department of Mechanical Engineering University of Ulsan, Ulsan, 44610, South Korea

Abstract: The planetary and interplanetary missions utilizing EP between 1993-2016 included demonstrations of Ion Thruster systems, Ion Thruster became more dominant as mission heritage was gained and as newer player we were developing our first version of RF Ion Thruster named iU-50. A 0-D analytical model of the plasma discharge was previously developed without magnetic ring-cusp ion engine based on energy and particles balance equations for predicting RIT thruster discharge chamber performance and thruster efficiency improvement which are affected by the design process including geometry of the discharge chamber, ion optic, RF coil and Gas inlet. The improved analytical model plays a critical role in estimating performance of iU-50. The present model is expanded by covering the secondary electron emission from the wall and the screen grid, double ionization xenon, Clausing factor and ion confinement factor produced by the induced electromagnetic field. In sum, several factors lead to a better calculation results that are verified by experiment data. The numerical results of our model were used as the first assumption for 2-D model by using PIC-DSMC simulation. By doing so, iU-50 is expected to produce a thrust and Isp of about 5 mN and 2600s at 2 sccm and 50 W of power.

Nomenclature

A	=	surface area, m^2
A_w	=	dielectric wall area, m^2
A_s	=	screen grid area, m^2
A_g	=	opening area of the screen grid, m^2
M_{xe}	=	mass of xenon, kg
m	=	mass of electron, kg
n_o	=	number density of neutrals, m^{-3}
n_i	=	number density of ions, m-3
P_{total}	=	total power input, W
T_e	=	electron temperature, eV
v_e	=	velocity of electrons, m/s
v_B	=	Bohm velocity, m/s
v_o	=	neutral gas velocity, m/s
T_a	=	grid optical transparency
f_c	=	ion confinement factor
I_B	=	Bohm current, A
I_s	=	ion current towards the screen grid, A
I_{total}	=	total ion current leaving the bulk plasma, A
I_b	=	beam current, A

[1] Professor, Department of Mechanical Engineering, jshin@ulsan.ac.kr.
[2] Student, Department of Mechanical Engineering, ptdquang.gt03@gmail.com.
[3] Student, Department of Mechanical Engineering, khonglinhtu2910@gmail.com

ϕ	=	plasma potential, eV
η_C	=	Clausing factor
γ	=	secondary electron yield
Q_{esc}	=	neutral gas escaping through the grid system, s-1
Q_{in}	=	gas injected into the discharge chamber, s-1
α_m	=	coefficient related with doubly-ionized ions
η_m	=	mass utilization efficiency

I.Introduction

Electric propulsion system using Hall thrusters or gridded ion thrusters has been developed and successfully utilized for space missions over several decades (Ref. 1-5). The development has not only been focused on the types of plasma thrusters but also on the size or power of the thrusters. Recent interest seems to focus on small size thrusters for micro or nano-scale satellites that are in a growing need (Ref. 6-8) owing to the advantages such as low launch cost with better redundancy (Ref. 9). However, as thruster size is reduced, efficiency drops significantly due to wall interaction. One option that can be chosen for micro-scale plasma thruster is RF gridded ion thruster. Advantage of RF ion thruster over DC ion thruster is the absence of a thermionic electron emitter which can limit a life-time of the satellite. Grid erosion by electrons impinging from the cathode can also be avoided. With reduced wall interactions, a scale-down can be feasibly made for RF ion thrusters. Plasma thrusters are usually designed, tested, and optimized for individual thruster. Hence it is helpful to have a better understanding of the detailed physics without spending considerable time and budget in the initial design phase of the new thruster. This usually relies on complicated numerical simulation (Ref. 10-12). However, it is very useful to predict the thruster performance with reasonable accuracy through simple steps in order to quickly assess the effect of various design and operating conditions. Goebel (Ref. 13) suggested a zero-dimensional analytical discharge model that can be used to predict the performance of RF ion thruster. Even though it did not consider the effect of one-dimensional field distribution that needs more sophisticated numerical simulation (Ref. 14) it provided a good estimation of the performance of RF ion thruster with a reasonable accuracy. Chabert et al. (Ref. 15) reported that the analytical modeling can improve the result by considering power transfer efficiency. Kanev. et al. (Ref. 16) applied the analytical model to cylindrical and semi-spherical discharge vessels. However, because the model did not consider some important physical phenomena in RF discharge such as magnetic field in RF ion thruster, the result was still not very accurate to predict the performance of RF ion thruster in some operational regime. In addition, most previous analytical models have been applied to large size RF ion thruster. Therefore, the analytical model needs to be further improved for evaluating the performance of small size thrusters. In this paper, we have tried to improve the zero-dimensional analytical model by taking into account more physical phenomena that occur in the RF ion thruster such as ion confinement effect caused by magnetic field and non-constant Clausing factor. Secondary electron emission and doubly-ionized xenon ions are also considered. Ion optics transparency which accounts for a fraction of escaped ions through grid system was also evaluated. The improved analytical model was compared to the results of reference analytical modeling and experiment.

II.Analytical modeling

In this paper, we extend the Goebel's model by introducing the secondary electrons emission from the wall and the screen grid, double ionization xenon, Clausing factor and ion confinement factor produced by the induced electromagnetic field for discharge chamber of RF gridded-ion Thruster. The key information about thrust performance (power absorbed, thrust, specific impulse, thrust efficiency, power efficiency) is found from plasma parameters consist of neutral gas density, electron temperature, plasma potential, ion and excited neutral production rates based on energy and particles balance equations into the discharge chamber. Geometry of the discharge chamber, ion beam current, parameters of the ion optic (transparency of girds) and gas flow rate are used as input parameters in the model. This paper is structured as follows: Sec. II the model is described in detail. Sec. III presents results and from calculation. A conclusion is given in Sec. IV.

A. Description of the Model

This section shows the implementation of the analytical model focusing on the input and the output parameters. For the sake of simplicity, consider first plasma chamber geometry including volume $\mathrm{V_{plas}} = \frac{1}{3}\pi(\mathrm{r_1^2} + \mathrm{r_2^2} + \mathrm{r_1 r_2})\mathrm{h}$ and the wall area is s $\mathrm{A_w} = \pi(\mathrm{r_1} + \mathrm{r_2})\mathrm{l} + \pi\mathrm{r_2^2}$. Figure 1 shows a schematic configuration of typical RF ion thruster and pathways of particle species considered in the analytical model. The helical RF coil wrapped around cylindrical dielectric casing can be modeled as a uniformly distributed N-turn solenoid coil. The typical driving frequency for RF ion thruster is about 3 MHz or lower and is inversely proportional to the diameter of the discharge chamber. The analytical model solves zero-dimensional charge conservation and energy conservation. The ion flux from the RF discharge consists of the fluxes towards the dielectric wall (I_w),the positive screen grid(I_{scr}) and through the grid aperture (I_b).

The electron temperature is calculated by balancing the production of Xe+ and Xe++ in Maxwellian plasma and their losses caused by wall-directed fluxes. Secondary electron emission from the dielectric surface can occur, which can reduce the sheath potential and increase the power loading in plasma thrusters (Ref. 17). RF plasma is quite uniform inside discharge chamber but there is weak dimensional dependence except for near wall. In view of the fact that the plasma remains quasi-neutral, $n_i \approx n_e$, any rapid spatial change in potential occurs in the space charge sheath rather than in the plasma. Additionally, in the RF Ion Thruster with dielectric wall, the power loss due to electron and ion entering toward the wall through the rf sheath represents the most significant power loss. The power loss to the wall can be estimated from the sheath potentials in the plasma edge. In the RF Ion Thruster, the wall is insulating, so the net ion and electron currents to the surface must be equal. Additionally, the energies characteristic of hall thrusters produces a significant number of secondary electrons through insulator materials, such as alumina (Al_2O_3), which reduces the sheath potential and increases the power loading in the plasma. Calculations of the electron temperate in the reference RF Ion Thruster ESA XX (Ref. 18). By equating the ion production and loss terms in the discharge chamber corresponding to the ion current from 0.78 – 2 Amps show electron temperature well in range of 0-20 eV. Secondary electron yields reported in the literature (Ref. 19-21) for several materials used for the walls of RF Ion Thruster are defined by the secondary electron yield $\gamma = \Gamma(2+b)aT_{eV}^{b}$, where the electron temperature is in electron volts, the gamma function is Γ(x) and the parametric constants, a and b for the solid surfaces are summarized in Table 1.

Table 1. Parametric constants for secondary emission [21].

material	a	b	$\Gamma(2+b)$
alumina (Al_2O_3)	0.145	0.650	1.49
stainless steel	0.040	0.610	1.44

The transparency for neutral propellant that leaks through the grids is β_g with $0 \le \beta_g \le 1$. Therefore, the open area of the grid system is $A_g = \beta_g \pi R^2$ and then no gas leaking out the volume ($\beta_g = 0$). At the uniform plasma inside the discharge chamber, the total ion loss area is $A_t = A_{scr} + f_c * A_w + A_{bw}$, where f_c and A_{bw} are the confinement factor that accounts for the reduction of ion current to the wall by magnetic field and back wall area respectively.

B. Charge and power balance in discharge chamber

In the thruster, only electrons have sufficient energy to overcome the potential difference between the plasma and the wall, whereas, ions fall from the plasma potential to the discharge chamber wall. The total discharge power that is needed to generate plasma is a sum of different power losses, which is given by:

$$P_{Total} = P_{coll} + P_{ion} + P_{elec} \tag{1}$$

Where P_{coll} is the collisional power loss which is a sum of singly ionization cost P_{i+} as following:

$$P_{i+} = n_0 n_e e \langle \sigma_i^+ v_p \rangle V_{plas} U^+ \tag{2}$$

and the excited neutral production loss P_{exc} is given by:

$$P_{exc} = \sum_j n_o\, n_e e \langle \sigma_{exc} v_e \rangle_j V_{plas} U^{exc} \tag{4}$$

Where v_e is the electron velocity, v_p is the primary electron velocity. The term in the brackets is the reaction rate coefficient calculating by averaging the single ionization, double ionization and excitation cross sections, that of σ_i^+, σ_i^{++} and σ_i^*, respectively, over the Maxwellian energy distribution. Ionization rate for Xenon could be approximated by such formula

$$\langle \sigma_i^+ v_p \rangle = 5 \times 10^{-14} \exp\left(-\frac{U^+}{T_{eV}}\right) T_{eV}^{0.5} \tag{5}$$

Double ionization rate with

$$\langle \sigma_i^{++} v_p \rangle = 2 \times 10^{-14} \exp\left(-\frac{U^{++}}{T_{eV}}\right) T_{eV} \tag{6}$$

And excitation rate could be approximated as following

$$\langle \sigma_{exc} v_e \rangle = 1.5 \times 10^{-16} \exp\left(-\frac{U^{exc}}{T_{eV}}\right) \tag{7}$$

Where $U^+$is the single ionization potential, U^{++} is the double ionization potential and U^{exc} is the average excitation potential. These value for Xenon is shown in the Table 2.

Table 2. Xenon propellant energy properties.

Types of ionization	Voltage
U^+ is the single ionization potential	12.13 eV
U^{++} is the double ionization potential	21.2 eV
U^{exc} is the average excitation potential	10.1 eV

In addition, the loss of accelerating charge across electric fields in the plasma sheath is by far the most popular of these power losses, which is made of ion loss and electron loss at the wall, screen grid and that is needed to generate a beam current I_b. The energy of the ions at wall is the sum of the ions fall through the preheat potential $T_{eV}/2$ and the acceleration of ions across electric fields in the plasma sheath with ϕ as following

$$\varepsilon_i = \frac{T_{eV}}{2} + \phi \tag{8}$$

The loss of accelerating ions to the discharge chamber is the sum of the loss of accelerating ions to the walls, the loss to the screen grid and the power needs generate a beam current I_b, which is given by

$$P_{ion} = (I_s + I_w + I_b)\left(\frac{T_{eV}}{2} + \phi\right) \tag{9}$$

The energy of electrons, that overcomes the negative sheath at the wall, removed from the plasma by Maxwellian electrons is:

$$\varepsilon_e = 2T_{eV} + \phi \tag{10}$$

The loss of electron current I_e to the wall is given by

$$P_{elec} = I_e(2T_{eV} + \phi) \tag{11}$$

The total current produced I_{total} is equal to the number of ionized particles that consists of singly ionized particle production rate I^{+} and double particle production rate I^{++}. This number is equal to the total loss of ions at wall, screen grid and ions current leaving plasma from the discharge chamber through the optical grid system which is given as

$$I_{total} = I^{+} + I^{++} = I_w + I_{scr} + I_b \tag{12}$$

The total ion current to the discharge chamber wall is given by

$$I_w = \frac{1}{2} n_i e \sqrt{\frac{kT_e}{M_{xe}}} A_w f_c \tag{13}$$

The very detailed explanation of the derivation of the confinement factor f_c, from the induced B-field which reduce ion loss to the wall, presented in the next section. The ion current to the screen grid area A_{scr} trapping by the screen grid which is depended on the effective ion optics efficiency as:

$$I_{scr} = \frac{(1-T_{eff})}{2} n_i e \sqrt{\frac{kT_e}{M_{xe}}} A_{scr} \tag{14}$$

The ion beam current I_b passes through the effective transparency of the ion optics system $T_{eff} = I_b/I_B$ that is given by the Bohm current as

$$I_b = \frac{1}{2} n_i e v_e A_{scr} T_{eff} \tag{15}$$

Where n_i is an ion density inside the discharge chamber and $v_e = (kT_e/M_{xe})^{1/2}$ is the Bohm velocity.

C. Secondary electron emission

Secondary electron emission heating does not play a critical role in most low-pressure discharge. In contrast, at high pressure, especially in RF discharges, secondary emission plays a crucial role in plasma production and can also contribute substantially to electron heating. Moreover, secondary electron emission from the dielectric surface can occur, which can reduce the sheath potential and increase the power loading in plasma thrusters (Ref. 22). The discharge vessel is made by Alumina (Al2O3) which should release the secondary electron from electron bombardment at high electron temperature. By particle balance for three species, the electron current leaving the discharge chamber I_e is same the total current produced I_{total}, as follows

$$I_{total} = I_e - \gamma I_e = (1-\gamma) I_e \tag{16}$$

The total ion current leaving the plasma can be found by substituting Eq. (13), Eq. (14), and Eq. (15) into Eq. (12) as follows

$$I_{total} = \frac{n_i}{2} e \sqrt{\frac{kT_e}{M_{xe}}} (A_w f_c + A_{scr}) \tag{17}$$

The electron current leaving the plasma is the random electron flux times the Boltzmann factor as

$$\phi = (1-\gamma) \frac{kT_e}{e} \ln\left[\frac{A_w f_c + (1-T_{eff}) A_s}{A_w f_c + A_s} \sqrt{\frac{2M}{\pi m}}\right] \tag{18}$$

The electron temperature is found by the Eq. (12) as follows

$$\frac{n_i}{2} e \sqrt{\frac{kT_e}{M}} (A_w f_c + A_{scr}) = n_o n_e e \langle \sigma_i^+ v_e \rangle V_{plas} + n_e^2 e \langle \sigma_i^{++} v_e \rangle V_{plas} \tag{19}$$

The solution to (19) for the electron temperature is then found by iteration of this equation in the form of

$$\frac{2 n_0 V_{plas}}{(A_w f_c + A_s)} = \frac{\sqrt{\frac{kT_e}{M}}}{\langle \sigma_i^+ v_e \rangle + \frac{n_e}{n_0} \langle \sigma_i^{++} v_e \rangle} \tag{20}$$

D. Clausing factor

It is essential that the neutral gas density, n_0, is accurately calculated in the discharge chamber. Because the singly ionized particle production rate and the excited neutral production rate is generated from the neutral density and it also defines the magnitude of electron temperature. When the plasma is switched on, the neutral gas is unionized that would escape the chamber is

$$Q_{esc} = Q_{in} - \frac{I_B}{e} \tag{21}$$

The neutral gas escapes through the grid is given by

$$Q_{esc} = \frac{1}{4} n_0 v_0 A_g T_a \eta_c \tag{22}$$

The first order estimation is utilized to determine the grid optical transparency T_a as follows

$$T_a = \frac{1}{(1/T_{eff}) + (1/T_{accel}) - 1} \tag{23}$$

Where T_{accel} is the accelerator grid transparency. Farnell proposed the conventional relationship between the screen and the accelerator grid transparencies, that is, $T_{accel}/T_s = 0.36$, n_0 is the neutral gas velocity, A_g is the grid area, the neutral gas velocity is $v_0 = (8 k_B T_{eV} / \pi M_{xe})^{1/2}$ and a resistance defined by the Clausing factor η_c, Which defines the reduced conductance of the grids with finite thickness. This factor determines the molecule transmission probability through the ion optics and is found by dividing the incident molecular flux G integrated over the downstream grid surface (grid 2) by the total incoming flux J integrated over the upstream grid surface (grid 1) as follows:

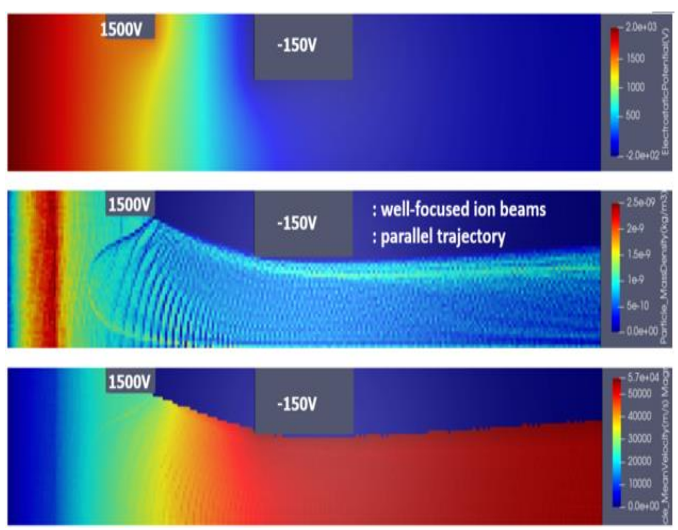

Figure 1. 2-D axisymmetric neutral gas density distribution normalized to the maximum value for ESA XX.

$$\eta_c = \frac{\int G dA_2}{\int J dA_1} \tag{24}$$

To calculate the Clausing factor, the Monte Carlo technique is used (Ref. 23). Besides, a single ion thruster aperture represented in a 2-D axisymmetric geometry is modeled using the molecular flow module in Vizglow by employing the angular coefficient method. The Clausing factor depends solely on the geometry of the grid system since it is nondimensional, regardless of the upstream neutral gas density. Using the model, we find that the Clausing factor for the ESA XX ion thruster ion optics grids is about 0.27. Vizglow also allows the neutral gas density distribution inside the aperture to be determined for a better understanding of how the ion optics arrangement constricts the neutral gas flow as shown in Fig. 2.

The neutral gas density inside the discharge chamber is calculated from the given beam current and mass utilization efficiency as follows

$$n_0 = \frac{4 I_B \alpha_m}{v_0 e A_g T_a \eta_c} \frac{\left(1 - \frac{\eta_m}{\alpha_m}\right)}{\eta_m} \tag{25}$$

It is assumed that singly charged ion and doubly charged ion exist together in the plasma. Using the equation of the thruster mass utilization efficiency, which is the ratio between the ionized and unionized propellant, for multiple species is given by

$$\eta_m = \frac{\dot{m}_1}{\dot{m}_p} = \alpha_m \frac{I_b M_{xe}}{e \dot{m}_p} \tag{26}$$

The mass flow input to discharge chamber is given by

$$\dot{m}_p = \alpha_m \frac{I_b}{e} \frac{M_{xe}}{\eta_m} \tag{27}$$

Where α_m is coefficient for a doubly charged ion in the beam current

$$\alpha_m = \frac{1 + \frac{1}{2} \frac{I^{++}}{I^{+}}}{1 + \frac{I^{++}}{I^{+}}} \tag{28}$$

Then, we set the neutral gas flow rate $\dot{m}_p$ in standard cubic centimeter per minute units as a boundary condition on the discharge chamber gas inlet surface area.

E. Ion confinement factor

The magnetic field induced by the RF coil depends on the coil size and amount of power from RF generator and matching network. For the simplest case, assume that the RF coil forms a solenoid and that the magnetic field inside a solenoid is

$$B[G] = 10^4 \mu_0 N I \tag{29}$$

Where μ_0 is the permeability of free space $\mu_0 = 4\pi \times 10^{-7}$ H/m, N is the number of turns per meter, and I is the coil current in Amperes. The Fig. 2 shows the effect of chamber configuration on the magnetic field. A copper coil AWG 12, 30 mm in length of coil, the number of turns is 15 was applied to the model. From the Fig. 2, the conical chamber has stronger field than cylindrical chamber. The filed has well-shape in the conical chamber.

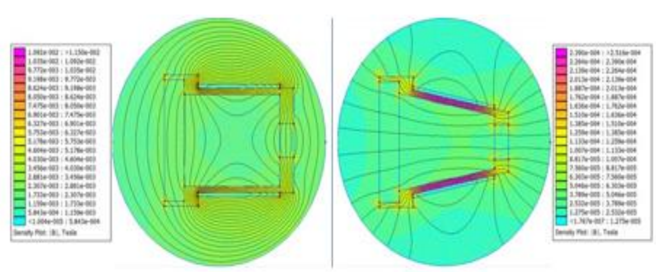

Figure 2. Effect of the discharge chamber configuration on the magnetic field (FEMM).

F. Energy consumption by plasma

The cost of producing ions is described by an ion production efficiency term, which is normally called discharge loss

$$\eta_{d\_loss} = \frac{P_{Total}}{I_b} \tag{30}$$

All parameters in equations are presented above, hence the discharge loss for RF ion thruster can then be calculated with easiness

$$\eta_{d\_loss} = \frac{2n_0 V}{\sqrt{\frac{kT_e}{M}} A_{scr} T_s}\left(\langle\sigma_i^{+} v_p\rangle U^{+} + \langle\sigma_i^{++} v_p\rangle U^{++}\right) + \left[\frac{(1-T_{eff})}{2} + \frac{A_w f_c}{A_{scr} T_s} + 1\right](2.5T_e + 2\phi) \tag{31}$$

III.Results and validation

Figure 3 shows the solution curves with various physical models for ESA-XX RF ion thruster with the beam current of 1.45 A and they are compared with reference experimental results (Ref. 24). and recent analytical modeling results (Ref. 16). The size of ESA-XX thruster is 26 cm in diameter and its power is 6.2 kW producing a thrust of 200 mN. It is shown in the Fig. 3 that the ion confinement effect produced by the magnetic field has the greatest effect on the results. When the Clausing factor (η_c) is changed from a fixed value (dashed curve) to a calculated variable value (dotted curve), the result gets closer to the experiment, especially at lower flow rates. When secondary electron emission is added (solid curve), the calculation results are mostly placed on the experiment values except at lower flow rates. The reason for the errors at lower flow rate is mainly because the error in loss terms especially the excitation loss calculated from the cross-section data becomes significant. In addition, the eddy currents that cause RF power losses on the screen grid is not considered in our model and the non-uniform distribution of the neutral density causes erroneous estimation of the wall-directed flux. Compared with reference analytical modeling result, it can be seen that the results of our analytical model that additionally takes into account various physical phenomena can better predict the thruster performance.

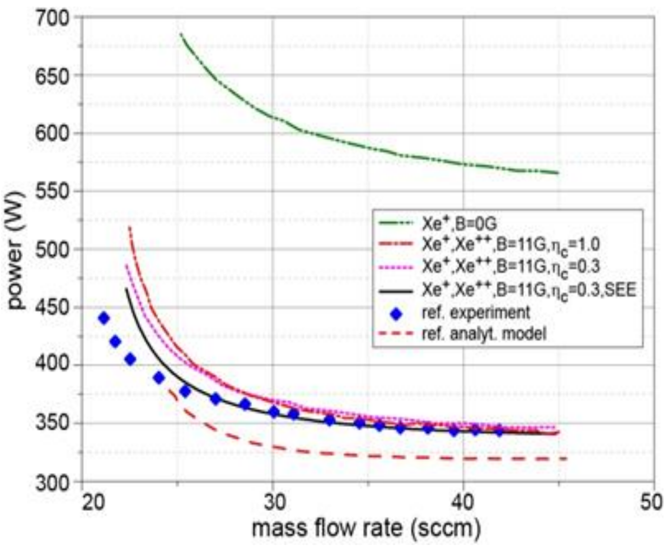

Figure 3. Comparison of the calculations obtained from the analytical models with various effects.

Figure 4 shows the curves of various loss components in the discharge for various mass flow rates. Calculation was performed for the same case presented in Fig. 2. The discharge is simply assumed to be sustained by a combination of volume ionization and surface loss. In RF ion thruster that has dielectric walls, the power loss due to the electron and ion currents that flow towards the dielectric walls through the RF sheath along the radial magnetic field and towards the screen grid shows the most significant power loss. On the other hand, the density structure of the plasma has little temporal modulation. The electron loss is much more than ion loss,

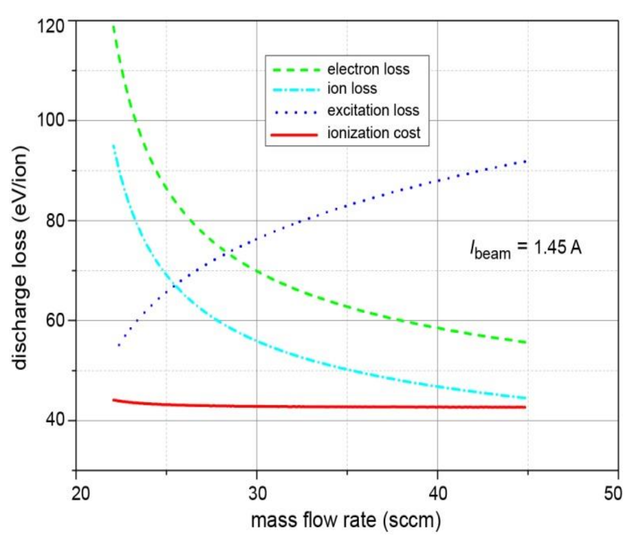

Figure 4. The ion production cost channels map of the ESA-XX RF ion thruster obtained by our analytical model at I_b = 1.45 A.

excitation loss or ionization cost. This is because the density profile of the ions in the sheath remains steady and the electrons are much more mobile. Hence, the electrons are able to respond virtually instantaneously, thereby changing the spatial extent of sheaths and quasi-neutral plasmas. For uniform plasma inside the discharge chamber, the total ion loss area is $A_t = A_g + f_c A_w + A_{bw}$, where A_g, A_w and A_{bw} are the opening area of the grid system, side wall area and back wall area, respectively. f_c is the reduction factor of Bohm current to the wall due to an AC magnetic field generated by the RF current flowing in the coil at RF oscillator frequency. Then, the power loss to the wall can be estimated from the sheath potentials in the plasma edge. As shown in the Fig. 4, the charge loss drops exponentially and the excitation loss increases as the flow rate increases. As flow rate increases, large portion of energy goes into the excitation of neutral gas. However, at lower flow rates, the charge loss becomes stronger because of the increased sheath potential and electron temperature. This results in higher ionization cost which demands significantly higher discharge power as shown in Fig. 2. The losses will increase in smaller size RF ion thrusters due to a larger area-to-volume ratio and reduced confinement factor. However, the excitation loss term becomes significantly smaller than other losses as the size of RF ion thruster decreases.

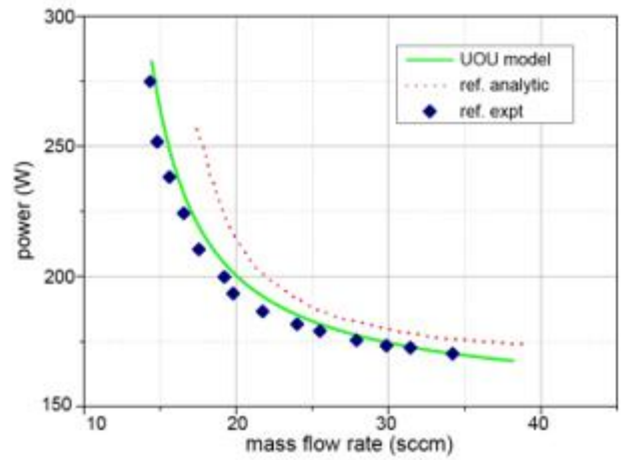

Figure 5. Experimentally and analytical obtained discharge power of the ESA-XX ion thruster in operation with ion beam current 780 mA 2-D axisymmetric neutral gas density distribution normalized to the maximum value for ESA XX.

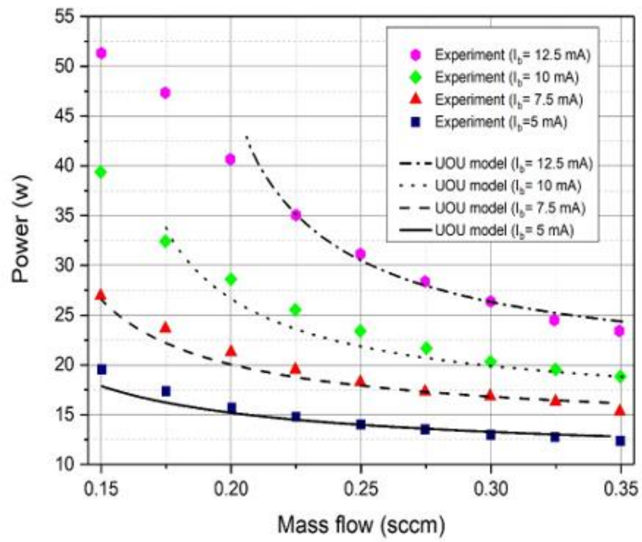

Figure 6. Comparision of our analytical model and experimental data at Vscr = 1250 V and Vdec = 150 V for the performance of RIM-4 RF ion thruster XX.

Figure 5 shows the discharge power curves for ESA-XX RF ion thruster with the beam current of 780 mA which is lower than 1.45 A presented in Fig. 2. Diamond curve corresponds to the experiment data (Ref. 24). and solid and dotted curves correspond to the calculation of our analytical model and the calculation result from (Ref. 16). respectively. The overall trend is the same as in high beam current case shown in Fig. 2. Figure 4 shows that our analytical model predicts experimental results better than reference model. More importantly, our analytical model produces a better agreement with experimental results even at lower flow rates. The calculation results presented in Fig. 2 and Fig. 4 confirm that our analytical model is acceptable to use for predicting the performance of large RF ion thrusters over various power ranges.

Our analytical model has also been validated for small RF ion thrusters and compared with experimental results. Figure 6 shows the power requirement for various beam currents as a function of mass flow rate compared with experimental results for RIM-4 ion thruster whose diameter is 4 cm with spherical discharge chamber (Ref. 25). It can be seen that even in small size micro thrusters, the calculation result provides good agreement with experimental result for various beam currents and powers. At low flow rates, however, the deviation from experiment becomes larger as noticed in Fig. 2.

Figure 7 shows the discharge loss calculated for RIM-4 RF ion thruster at fixed mass utilization efficiency of 90%. In this case, the ion beam current is adjusted to match the target mass utilization efficiency. For a given beam current, the mass flow rate that produces specific mass utilization efficiency can be uniquely determined. Unlike shown in the previous curves where the discharge loss decreases as the mass flow increases, there exists an optimal mass flow rate for which the discharge loss becomes minimum. For this RIM-4 RF ion thruster, the minimum loss occurs at beam current of 12.5 mA at 90% mass utilization efficiency. A similar behavior is also obtained for larger RF ion thrusters.

Figure 8 shows performance map calculated for a family of micro-scale RF ion thrusters of RIT-1, RIT-2, RIT-3, RIT-4, RIT-10, and RIT-15 and compared with the measurement points (dot points) which were taken from (Ref. 26-27). The number given in each thruster name indicates the approximate beam diameter. The beam current used for the calculation of each thruster was chosen from the reference. It is noted that the performance curves obtained from the calculation intersect with the measurement points for all RITs considered. It can be inferred from Fig. 5 and Fig. 7 that our analytical model provides a robust prediction of the performance over a wide range of micro-scale RF ion thrusters.

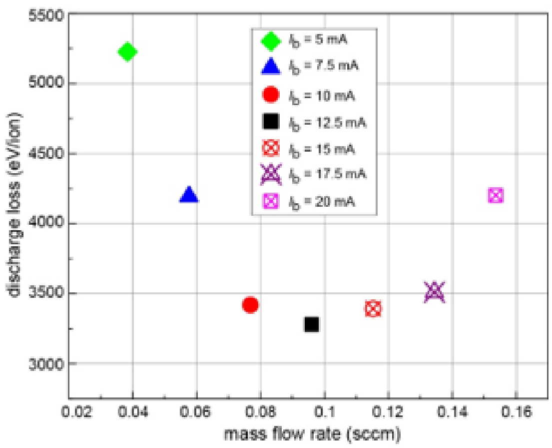

Figure 7. Discharge loss calculated for RIM-4 RF ion thruster at a fixed mass utilization efficiency of 90 % for various ion beam currents.

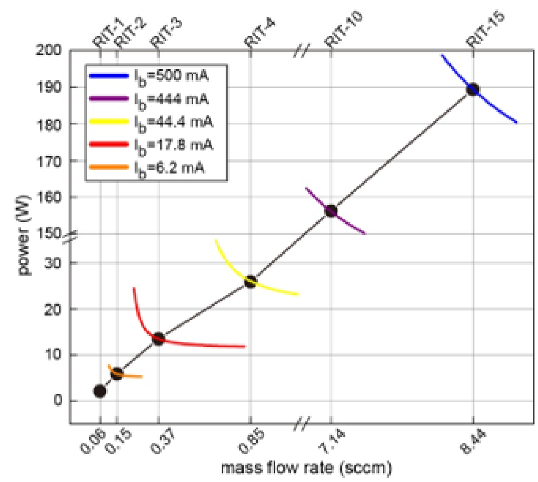

Figure 8 Performance map of a RIT ion thruster family obtained by our model and experimental data at various of the ionizer diameter and RF-frequency with different xenon propellant flow rate.

IV.Summary and conclusion

In the design phase of the RF ion thruster, a quick and accurate prediction of the performance can be very useful. This study has further improved the previously reported analytical model for RF gridded-ion thruster to provide better predictions. The additional physical models we considered were 1) secondary electrons emission, 2) double ionization, 3) effective ion optics transparency, 4) variable Clausing factor obtained by the Monte Carlo calculation, and 5) ion confinement factor generated by the electromagnetic field in the discharge chamber. Among them, the ion confinement factor had the greatest effect on the calculation, while other effects made some minor corrections especially at lower flow rates. The calculation results obtained from our improved analytical model were in a good agreement with experimental results for both large and small RF ion thrusters with various beam currents and powers.

V.Acknowledgments

This work was supported by the 2017 Research Fund of University of Ulsan, South Korea.

References

[1] Lev D, Myers R, Lemmer K, Duchemin O. 2017, Proceedings of the 35th IEPC, 242

[2] Choueiri E Y. 2004, Journal of Propulsion and Power, 20: 193

[3] Mazouffre S. 2016, Plasma Sources Science and Technology, 25: 033002

[4] Jahn R G, Choueiri E. Y. 2002, Electric Propulsion, Encyclopedia of Phys. Sci. and Technol. 3rd Ed., 5, New York, Academic Press

[5] Killinger R, Leiter H, Kukies R. 2007 RITA Ion Propulsion Systems for Commercial and Scientific Applications, 43rd AIAA/ASME/SAE/ASEE Joint Propulsion Conference & Exhibit, AIAA Paper, 2007-5200

[6] Tsay M, Hohman K, Olson L. 2009, 23rd Annual AIAA/USU, SSC09-II-1

[7]Martinez-Sanchez M, Pollard J E. 2007, Journal of Propulsion and Power 14: 688
[8] Lev D, Myers R M, Lemmer K M, et al. 2017, Proceedings of the 35th IEPC, 242
[9]Wirz R E. 2015, Proceedings of the 34th IEPC, 275
[10] Henrich R, Becker M, Heiliger C. 2017, Proceedings of the 35th IEPC, 518
[11]Arzt T. 1988, Journal of Physics D: Applied Physics, 21: 278
[12] Tsay M. 2010, Two-Dimensional Numerical Modeling of Radio-Frequency Ion Engine Discharge. Ph. D. Thesis, MIT
[13] D. M. Goebel. 2008, IEEE Transactions on Plasma Science, 36: 2111
[14] Dobkevicius M., Feili D. 2017, Journal of Propulsion and Power, 33: 939
[15] Chabert P, Arancibia Monreal J, Bredin J, et al. 2012, Phys. Plasma, 19: 073512
[16] Kanev S V, Khartov S A, N0069gmatzyanov V V. 2017 Proc. Engineering, 185: 31
[17] Raitses Y, Smirnov A, Staack D, et al. 2003, Physics of Plasma, 13: 014502
[18]File J M, Martinez-Sanchez M, Szabo J. 1997, Proc. 33rd Joint Propulsion Conf., p.3052
[19] Bugeat J P and Koppel C. 1995, Proc. 24th IEPC, p. 286
[20]Gascon N, Dudeck M, Barral S. 2003, Phys. Plasma. 10: 4123
[21]Goebel D M, Katz I. 2008 Fundamentals of Electric Propulsion: Ion and Hall Thrusters, ed. JPL (California) Chap. 7
[22] Chabert P, Braithwaite N. 2011, Physics of Radio-Frequency Plasma, ed. Cambridge University (Cambridge) Chap. 1
[23] Bohm B. 1949, The Characteristics of Electric Discharges in Magnetic Fields, New York, McGraw-Hill, pp. 1-763
[24] Bassner H, Bond A R, Thompson K V, et al. 1997, Eur. Space Agency ESA SP-398, p. 251
[25] Volkmar C, Ricklefs U. 2015, Eur. Phys. J. D, 69: 1
[26] Bassner H, Bond A R, Thompson K V, et al. 1997, Eur. Space Agency ESA SP-398, p. 251
[27] Volkmar C, Ricklefs U. 2015, Eur. Phys. J. D, 69: 1